Bio-Design and Manufacturing (2019) 2:161–171
https://doi.org/10.1007/s42242-019-00046-7

RESEARCH ARTICLE

3D printing of calcium phosphate bioceramic with tailored biodegradation rate for skull bone tissue reconstruction

Boqing Zhang[1] · Huan Sun[1] · Lina Wu[1] · Liang Ma[3] · Fei Xing[2] · Qingquan Kong[2] · Yujiang Fan[1] · Changchun Zhou[1] · Xingdong Zhang[1]

Received: 12 July 2019 / Accepted: 31 July 2019 / Published online: 22 August 2019

Abstract
The bone regenerative scaffold with the tailored degradation rate matching with the growth rate of the new bone is essential for adolescent bone repair. To satisfy these requirement, we proposed bone tissue scaffolds with controlled degradation rate using osteoinductive materials (Ca-P bioceramics), which is expected to present a controllable biodegradation rate for patients who need bone regeneration. Physicochemical properties, porosity, compressive strength and degradation properties of the scaffolds were studied. 3D printed Ca-P scaffold (3DS), gas foaming Ca-P scaffold (FS) and autogenous bone (AB) were used in vivo for personalized beagle skull defect repair. Histological results indicated that the 3DS was highly vascularized and well combined with surrounding tissues. FS showed obvious newly formed bone tissues. AB showed the best repair effect, but it was found that AB scaffolds were partially absorbed and degraded. This study indicated that the 3D printed Ca-P bioceramics with tailored biodegradation rate is a promising candidate for personalized skull bone tissue reconstruction.

Keywords 3D printing · Skull repair · Calcium phosphate ceramics · Tailored biodegradation rate · Bone reconstruction

Introduction

The skull is a highly personalized bone tissue. Ideal skull repair and reconstruction implants are needed further explored. For children or adolescents, the inert implants used by adults are not suitable for this condition since their bone tissues are growing up. Osteoinductive biodegradable implants may be a good solution for this case. With the improvement of people's health level, patients are currently not satisfied with the use of traditional bone orthopedic implants to restore basic shape restoration but to reconstruction of their skulls. This requires new generation of biomaterials with accurate shape to match the defect and tailored biodegradation rate to support bone regeneration [1]. Calcium phosphate (Ca-P) shows good osteoconductive and osteoinductive and is a promising bone repair biomaterial owing to their similar composition to normal bone [2–5].

Ca-P ceramics with suitable pore structure and composition were found to be osteoinductive under certain circumstances. Zhang et al. [6] reported that their synthetic porous Ca-P ceramics induced osteogenesis in a non-bone environment, and later explored the mechanism of induced osteogenesis. At present, the international academic community has reached a consensus on the osteoinductivity of Ca-P ceramics, which promotes the application of Ca-P ceramics in clinical medicine. Ca-P with different compounds has been successfully synthesized in the laboratory. As the calcium phosphate ratio (Ca/P) decreases, the solubility and hydrolysis rate of calcium phosphate salt increased; therefore, only optimized Ca/P composition ceramic is suitable for implantation [7]. Hydroxyapatite (HA) is very similar in composition to the inorganic matter of human bones, but it dissolves very slowly in the body [6, 8]. Ripamonti et al. reported that the porous HA ceramics using coral reefs and implanted into the muscles of the iliac crest observed bone induction phenomenon [9]. Tricalcium phosphate (TCP) has

✉ Liang Ma
liangma@zju.edu.cn

✉ Changchun Zhou
changchunzhou@scu.edu.cn

1 National Engineering Research Center for Biomaterials, Sichuan University, Chengdu 610064, China

2 Department of Orthopedics, West China Hospital, Sichuan University, Chengdu 610041, China

3 State Key Laboratory of Fluid Power and Mechatronic Systems, School of Mechanical Engineering, Zhejiang University, Hangzhou 310058, China

two crystal phases: α- and β-tricalcium phosphate (TCP) [10]. β-TCP showed better biological activity and become the popular bone substitute biomaterials. β-TCP possesses a Ca/P ratio of 1.5, which is more soluble than HA [11, 12]. Although β-TCP shows a higher dissolution rate, it is difficult to retain a temporary mechanical support for the desired duration of implantation. Yuan et al. prepared α-TCP and β-TCP ceramics with the same macroscopic structure and microstructure, and implanted them into the dorsal muscle of the dog. It was found that only β-TCP ceramic formed new bones inside the scaffolds [13]. HA has good biological activity, but it showed poor biodegradation rate in vivo. β-TCP has good degradability, but it showed poor mechanical properties. Therefore, a large number of studies have been investigated combining β-TCP and HA together, i.e., the biphasic calcium phosphate ceramics (BCP), which have better biological properties than HA or β-TCP alone [14–18]. By controlling the composition ratio and preparation conditions of the material, BCP with suitable degradation rate can be tailored. The degradation rate of BCP depends on the ratio of HA and β-TCP. The higher the ratio of β-TCP, the better the degradability.

In bone tissue engineering, the bone repair materials only need to mimic the chemical composition of the natural bone, but it is also needed to achieve the desired degradation rate. The chemical composition and the porous structure of the scaffolds determined the bioactivity of the material [8, 19–24]. Complex porous structures scaffolds are difficult to obtain via conventional fabrication process [25]. In the past two decades, a lot of porous scaffolds fabrication methods have been reported; for example, freeze-casting [26, 27], addition of porogen [28, 29], gas foaming method [30–32] and directional crystallization method [33] were widely studied. The above techniques showed some shortcomings; for example, it is difficult to customize internal pore structure. It is difficult to prepare a transplant with a complex shape. Three-dimensional (3D) printing technologies show better ability to control the porosity of the scaffolds [34, 35]. By using the 3D printing technologies, it is very easy to control the composition and the porous structure of varied bone tissue scaffolds. It was reported that this 3D printing technologies have been successfully used to make different types of bone tissue implants [3, 36–38].

It is clear that a biodegradable scaffold after implantation is intimately connected with its new bone regeneration and biodegradation. Therefore, it is crucial to explore a new type of controllable degradation rate scaffold to reconstruct the adolescent bone repair. In this study, we proposed calcium phosphate scaffolds with tailored biodegradation rate by using 3D printing technology. The degradation rate of the calcium phosphate scaffold is controlled by adjusting the composition and porous structures of the scaffold, which are expected to achieve a balance between biodegradation of scaffold and new tissue growth. A simple animal model was proved on the beagle skull repair. It indicated that the 3D printed Ca-P bioceramics with tailored biodegradation rate is a promising candidate for personalized skull bone tissue reconstruction.

Experimental

Materials

Calcium phosphate powders (HA, β-TCP, BCP) were purchased from National Engineering Research Center for biomaterials (Chengdu, China). PVB (polyvinyl butyral, Mn = 70,000–90,000), ethanol (AR), PVA (polyvinyl alcohol) and PEG (polyethylene glycol PEG-2000) were purchased from sigma. The printing ink was prepared by mixing PVB, calcium phosphate powders and ethanol in a ratio of 3.6:32:32. The ink was continuously stirred in open environment to maintain powders distribution and increase the viscosity by solvent evaporation until ideal viscosity for 3D printing.

Tailored Ca-P bioceramic biodegradation rate by 3D printing

The scaffolds (3DS) were prepared by an inkjet 3D printing device (ALPHA-BP11, Beijing Sunp Biotech). The printing inks were prepared by calcium phosphate powders. The diameter (d) of the nozzles was between 110 and 800 μm, and the slice layers thickness (h) was varied according to the diameter of the nozzle, following an empirical formula: $h = 0.8d \pm 0.02$ μm. The speed of nozzle was between 240 and 600 mm/min during 3D printing. The distance between the two filaments was set between 500 and 1400 μm. The model of the specimen was generated by 3D molding software. The model data were transferred to stereolithography (STL) format which most 3D printers are acceptable for printing. The inner pore sizes were designed by slicing software. Printing strategy adopted orthogonal porous structure mode. After previous layer printing was completed, the nozzle moved upward and continued to print next layer with direction vertical to previous filaments. The 3D printing process for fabrication of calcium phosphate scaffolds with tailored biodegradation rate is shown in Fig. 1a. The principle of adjusting the calcium phosphate scaffolds biodegradation rate is shown in Fig. 1b. The degradation rate of the calcium phosphate scaffold was controlled by adjusting the composition and porous structures. The Ca-P porous ceramics scaffolds fabricated by using conventional H_2O_2 foaming method (foaming scaffolds, FS) were used as the control group.

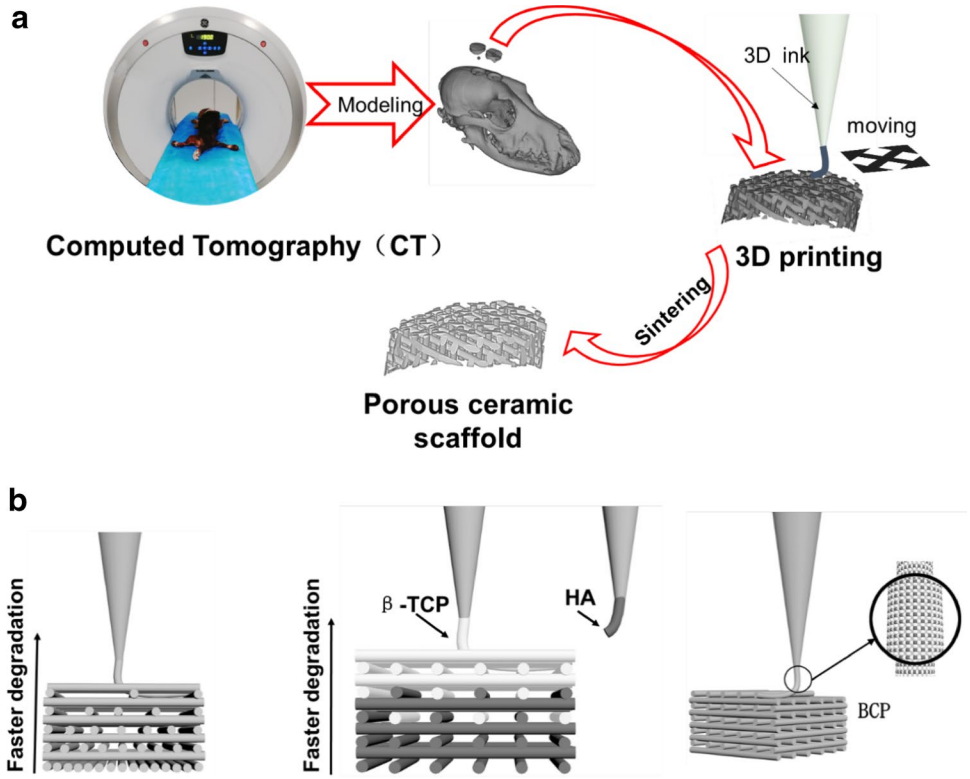

Fig. 1 **a** Schematic of printing calcium phosphate bioceramic with tailored biodegradation rate for skull bone tissue reconstruction. **b** The principle of adjusting the calcium phosphate scaffolds biodegradation rate

Post-treatments and sintering

After the specimens were printed, the specimens were dried for 4 h at temperature of 60 °C; then, the specimens were sintered in muffle furnace. Briefly, specimens were sintered by two-step sintering process. Firstly, specimens were heated by rate of 5 °C/min to 600 °C and hold for 2 h to evaporate polymer and form micropores. Then, specimens were heated to 1100 °C with same heating rate and hold time. Finally, specimens were cooled down to room temperature in the furnace.

Characterization of the tailored biodegradable Ca-P bioceramics

The morphology of the printed specimens was evaluated by scanning electron microscope (SEM, JSE-5900LV, Japan). The specimens and powders were sputter-coated with gold before observation. Phase composition of the scaffold was analyzed using XRD (Philips X'Pert 1 X-ray diffractometer, Netherlands) with Cu$K\alpha$ radiation at a current of 20 mA and voltage 30 kV. Scans were performed with 2θ values from 20° to 60° at a rate of 0.05°/s. The obtained peaks were compared with standard references in the JCPDS file available in the software for HA (09-0432) and β-TCP (09-0169). The mechanical properties of the printed specimens were tested with electronic universal testing machine. Standard test specimens which have different porosities were fabricated as cylinder with $\varphi 7 \times 12$ mm. Stress–strain curve of the scaffolds was performed at a crosshead speed of 1 mm/min, and compressive strength was generate by stress–strain curve. The force was loaded along the vertical direction of the pores. The shrinkage after sintering was measured by Vernier caliper.

In vivo experiments

Animal skull defect models

Beagles were obtained from the Sichuan University Laboratory Animal Center (body weight: 10–11 kg; gender: male). All the experiments were approved by the Animal Care and Use Committee of Sichuan University. The animals were anesthetized by intraperitoneally injecting 0.02 g/ml pentobarbital sodium before experimentation (40 mg/kg body weight; Sigma Chemical, St. Louis, MO, USA). The three-dimensional data of the skull of experimental animals were obtained by computed tomography (CT, Optima CT680, GE Medical, USA). Then, the 3D model of the skull was established by computer. And two round defects with a diameter of 15 mm of the skull were generated by modeling software to mimic a freeform bone defect. The shapes of defects were remolded by Boolean operation through Magics 22 (Materialise, Belgium).

Implantation experiments

The animals were anesthetized by intraperitoneally injecting 0.02 g/ml pentobarbital sodium before implantation (40 mg/kg body weight; Sigma Chemical, St. Louis, MO, USA). Then, two pre-designed bone defects on the skull of the experimental animal were prepared by surgeon team. The autologous bone (AB) taken from the defect site was used as a new repair material. The experiment consisted of two groups of beagles: one group was implanted with 3DS and FS scaffolds, and the other group was implanted with autologous bone (AB) and 3DS scaffolds. Triple parallel specimens were tested for each implantation. After implantation, the beagles were continuously injected with penicillin at 105 U/kg per day for 3 days to prevent infection. The specimens were harvested after 5 months of implantation by killing the beagles. The implanted specimens were extracted from the surrounding tissues and washed with a phosphate-buffered saline (PBS). The attached tissues were washed with a mixture of PBS (90 wt%) and pepsin (10 wt%). The harvested implants were then fixed in 10% formaldehyde in PBS solution for 2 weeks and then dehydration treatment. The dehydrated process was taken with a gradient of ethanol solutions (60%, 80%, 96%, 100%, 100%, ethanol/technovit 7200 VLC: 70/30, ethanol/technovit 7200 VLC: 50/50, ethanol/technovit 7200 VLC: 30/70, and technovit 7200 VLC: 100%) 1 day for each solutions, and in 100% technovit 7200 VLC for 1 week. The dehydrated samples were embedded in technovit 7200 VLC and light curing (Technovit 7200 VLC, Kulzer-Exakt, Wehrheim, Germany), and then mounted with resin onto sample holders suitable for an automated brushing machine (SD Mechatronik GmbH, Feldkirchen-Westerham, Germany). The embedded specimens were cut into 5 μm histological slides by using Leica Polycut (Leica, SM 2500E, Germany) and transferred to glass slides. The sections were stained with hematoxylin and eosin (HE) for histological analysis.

Result

Composition and phase analysis of 3D printed Ca-P ceramics

The composition and crystal phase of 3D printed Ca-P ceramics were further analyzed by X-ray diffraction (Fig. 2). The diffraction pattern for the specimen No. 1 has peaks at 31.8°, 32.9° and 32.2°, corresponding to (211), (300) and (112) of HA (JCPDS 09-0432), respectively. The diffraction patterns of the HA bioceramic only exhibited the characteristic lines and bands of HA. No secondary phase, organic residue or crystallographic substitution was detected. Specimen No. 4 showed sharp peaks at 31.0°, 34.3° and 27.8° and corresponded to (214), (0, 2, 10) and (220) which were characteristic of β-TCP (JCPDS 09-0169 β-TCP). It showed that pure β-TCP ceramics were prepared. In BCP (No. 2 and No. 3), the diffraction peaks of both β-TCP and HA were sharp and intense, indicating their highly crystalline nature. No impurity peaks were observed, which confirmed high purity of the two products. By quantitative calculation, specimen No. 2 and specimen No. 3 contained 70% and 30% β-TC, respectively.

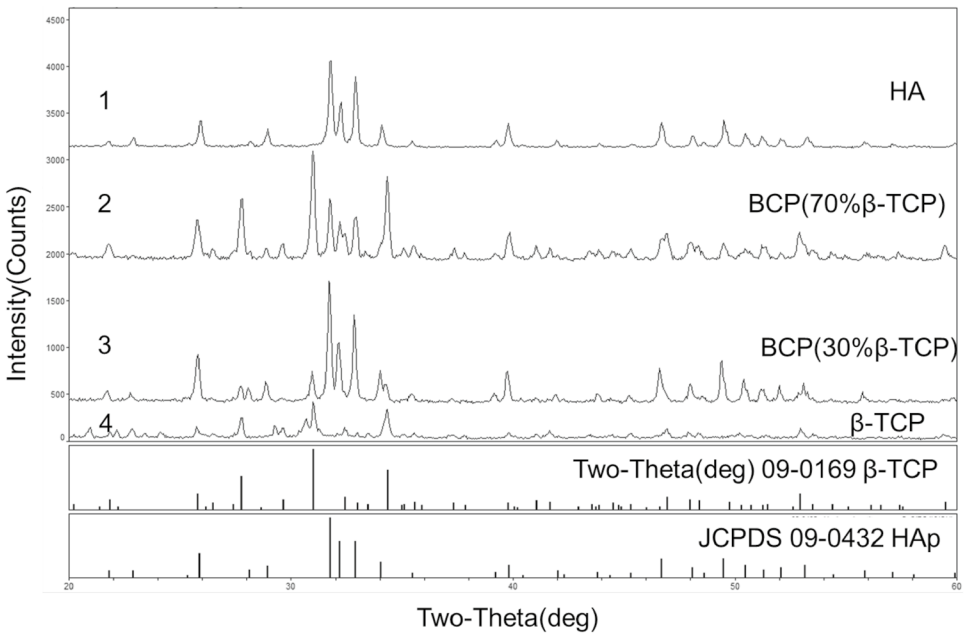

Fig. 2 The XRD patterns of different Ca-P ceramics

Morphology of tailored biodegradable Ca-P bioceramic

The scaffolds were fabricated in a cellular lattice structure using a 0°/90° lay down pattern with a continuous contour filament to ensure they have 3D porous spatial structure that mimic trabecular bone, as shown in Fig. 3a. Scanning electron microscope images displayed the microstructure feature features of the 3D scaffolds. The size of the pores in the scaffold was designed by Slicing software, according the requirements. These scaffolds have interconnected pores with diameters of 200 μm, 400 μm, 700 μm, respectively (Fig. 3b–d), which were pre-designed for different degradation rates. In addition, the porosity of Ca-P ceramics with different pore sizes was tested by theoretical formula method (Fig. 3e). It can be found that the porosity of Ca-P ceramics increased nonlinearly with increase in pore size. When the pore size was printed at 200 μm, the porosity was about 50%, and when the pore size was increased to 700 μm, the porosity was about 75%.

The mechanical property and shrinkage

The porosity of the scaffold significantly would affect the mechanical properties of the Ca-P scaffolds. The compressive strength was tested via an electronic universal machine. As shown in Fig. 4a, the compressive strength of Ca-P ceramics was decreased obviously, as increase in porosity. Specifically, when the porosities were 60%, 70% and 80%, the compressive strength was about 5.5 MPa, 3.0 MPa and 1.0 MPa, respectively. In order to accurately prepare a personalized repair scaffold, it needs to know the shrinkage

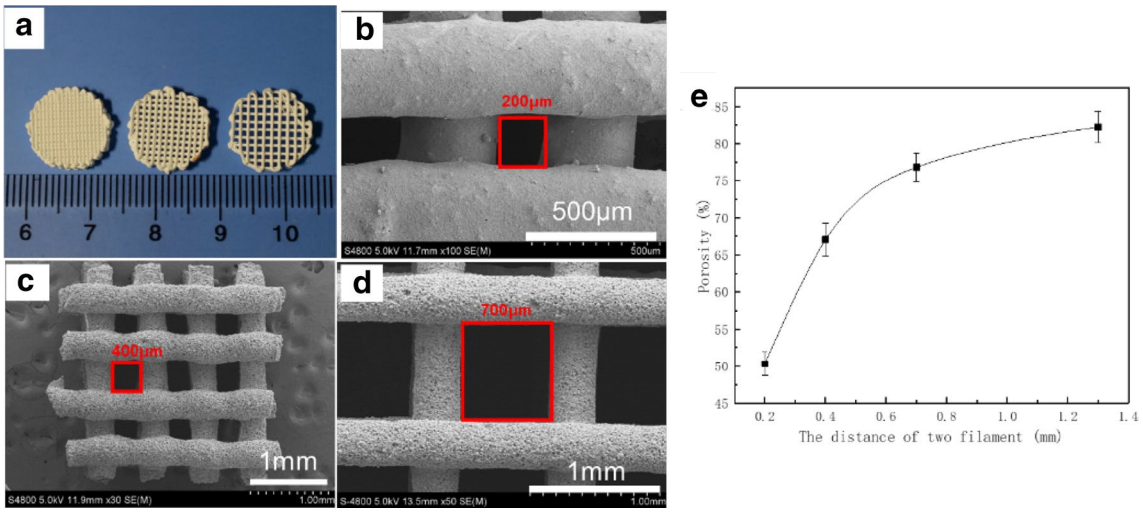

Fig. 3 Morphology and porosity of scaffolds with different pore sizes

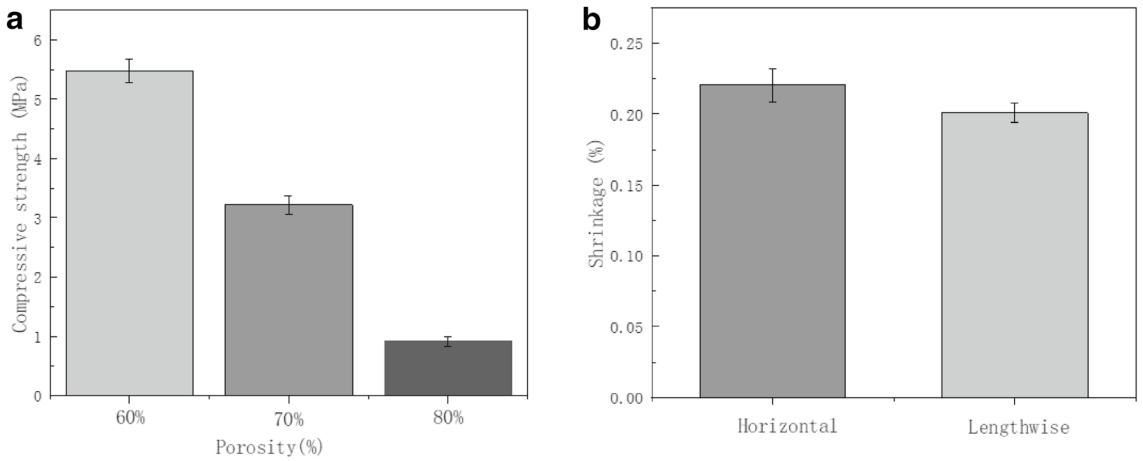

Fig. 4 **a** The compressive strength of Ca-P ceramic with different porosity. **b** The shrinkage of Ca-P ceramic scaffold after sintering

before and after sintering of the scaffold. The shrinkage of Ca-P ceramics was about 22%, and the shrinkage in horizontal was slightly greater than that in lengthwise (Fig. 4b).

Phase composition and biodegradation rate

Since the solubility and hydrolysis rate of the calcium phosphate increase, the ratio of calcium to phosphorus (Ca: P) decreases; therefore, optimizing the calcium phosphate phase composition is necessary for adjusting the biodegradation rate. The solubility of the Ca-P ceramic affects its degradability. As materials with different phase compositions show different solubility, phase composition partly affects the solubility of the Ca-P ceramics. Table 1 summarizes the Ca/P ratios and the aqueous solubility of several Ca-P phases, which can be used to predict the degradation of Ca-P ceramic in vivo. Among of them, HA was most stable and least soluble one ($K_{sp} \approx 6.62 \times 10^{-126}$), while β-TCP was the most unstable and it has the highest solubility (6.21×10^{-34}). The solubility of BCP was between HA and β-TCP, and increased with the increase in β-TCP content. According to the calculation of the content of phase, when the β-TCP content was 30%, its solubility would be 6.21×10^{-34}, but when the β-TCP content increased to 70%, the solubility increased significantly to 1.45×10^{-33}. Furthermore, the relative degradation rate of Ca-P ceramics in the same environment can be presumably predicted according to the right figures. It can be seen from the corresponding right figures that HA ceramics hardly degrade relative to another specimen in vivo. However, β-TCP ceramics possess the fastest degradation rate. BCP ceramic degradation rate was moderate between HA and β-TCP. Therefore, the Ca-P ceramic degradation can be further tailored for the different biodegradation rate.

Table 1 Ca/P ratios and the aqueous solubility of several Ca-P phases

Materials	Formula	Ca/P ratio	Solubility (K_{sp})
HA	$Ca_{10}(PO_4)_6(OH)_2$	1.67	6.62×10^{-126} [18]
α-TCP	$Ca_3(PO_4)_2$	1.5	8.46×10^{-32} [18]
β-TCP	$Ca_3(PO_4)_2$	1.5	2.07×10^{-33} [18]
BCP (30% β-TCP)	–	–	6.21×10^{-34}
BCP (70% β-TCP)	–	–	1.45×10^{-33}

The right image shows the relative degradation rate of Ca-P materials with different compositions

Beagle skull regeneration

In the past, a large number of studies have showed that calcium phosphate ceramics have good bone repair effects, but these results only prove the feasibility of calcium phosphate ceramics as bone repair materials. Actual clinical implants are much more complex, which includes acquiring, modifying and shaping of the implanted materials according defects that may vary widely in size and shape. Therefore, this study designed beagle personalized skull defect repair to procedure the actual surgical application. Figure 5a is the skull target model of the experimental animal, which was reconstructed from computed tomography (CT) data. A circular defect with a diameter of 15 mm was established at the apex of the skull, and the filling model of the defect was used as a target model to prepare a calcium phosphate porous scaffold by 3D printing. During the experiment, gas-foamed ceramics scaffold (FS), 3D printed scaffolds (3DS) and autologous

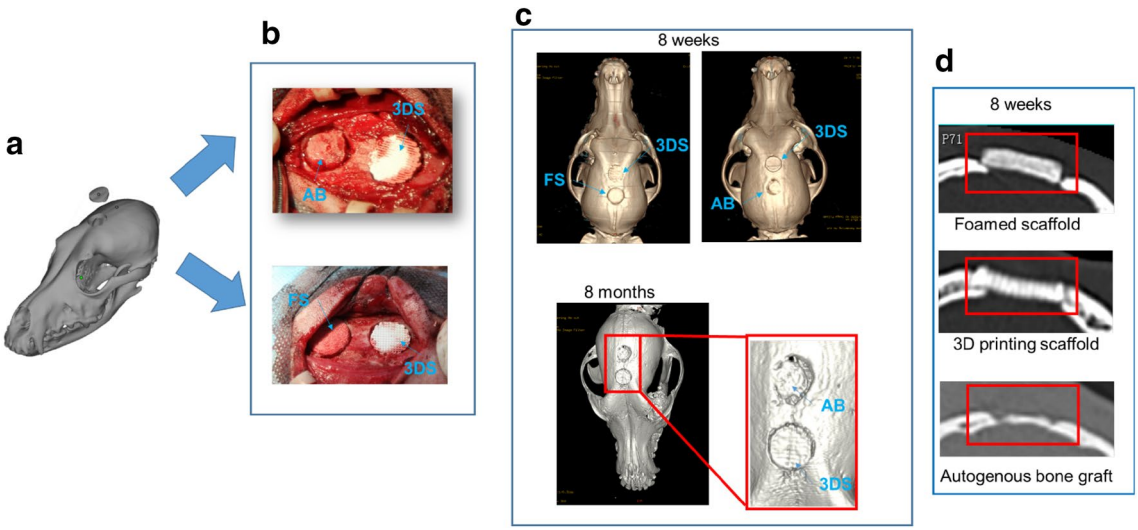

Fig. 5 The diagram of personalized beagles skull repair. **a** Skull model of the objective animal (a cycle defect with a diameter of 15 mm was designed). **b** Implantation of different scaffolds into beagle skull. **c** After 8 weeks and 8 months, 3D models of the beagle skull with different scaffolds. **d** After 8 weeks, the CT image of different scaffolds

bones (AB) were simultaneously implanted into the defect site (Fig. 5b). After 8 weeks of implantation, the experimental animals were scanned by CT technique and the 3D model was reconstructed, as shown in Fig. 5c. The 3DS and the FS were well integrated with the surrounding tissue, but the 3DS was more conformable to the original skull surface curve. In the enlarged CT image (Fig. 5d), a gap between the FS and the surrounding tissue is observed and the scaffold was higher than the original skull surface. In contrast, the 3DS was more suitable for the surrounding bone tissue. In the AB and 3DS repair, it was found that the 3DS and the surrounding tissue were tightly combined to have a good repair effect, while the AB showed bone resorption during the repair process. A slight collapse caused poor post-repair. This was also well confirmed in the CT image (Fig. 5d).

The AB and 3DS were observed for 8 months after implantation. The model with the reconstruction of the CT data is shown in Fig. 5b. By the time of repair to 8 months, the autologous bone was absorbed obviously, and the gap between the tissue and the surrounding tissue continuously increased. In contrast, 3DS showed better repair ability.

Histological observation and biological functions

In order to observe the internal bone ingrowth of different scaffolds, samples with a small amount of surrounding bone tissue repaired for 5 months were taken out (Fig. 6a). Hard tissue slices were made and stained with hematoxylin–eosin (HE) as shown in Fig. 6b–i. As shown in Fig. 6a, FS and 3DS were well combined with the surrounding tissue. From the overall splicing images of 3DS and FS repair (Fig. 6b, c, f, g), it can be found that FS has a series of pores of different sizes and a large number of new bone tissues have grown inside the pores. New bone tissue sticks to the wall of the pores and grows toward the core of the pore. Almost all the pores in the whole FS have new bones. 3DS has a regular pore structure, and all pores were basically of the same size and shape. Although there were fewer new bone tissues in 3DS, there observed new bone tissues in the core of the scaffold. It can be found that bone tissue grows internally along the surface of the scaffold. These results indicated that both 3DS and FS scaffolds can promote new bone regeneration, but 3DS provides versatile methods for customizing the shape of implants.

Vascularization in 3DS and FS

In bone tissue engineering, vascularization is an important indicator for evaluating bone repair potential. A large number of neovascularization in the soft tissue inside the scaffolds were found in H&E histological image (Fig. 7a–c). Some blood vessels were marked with red solid coils. In

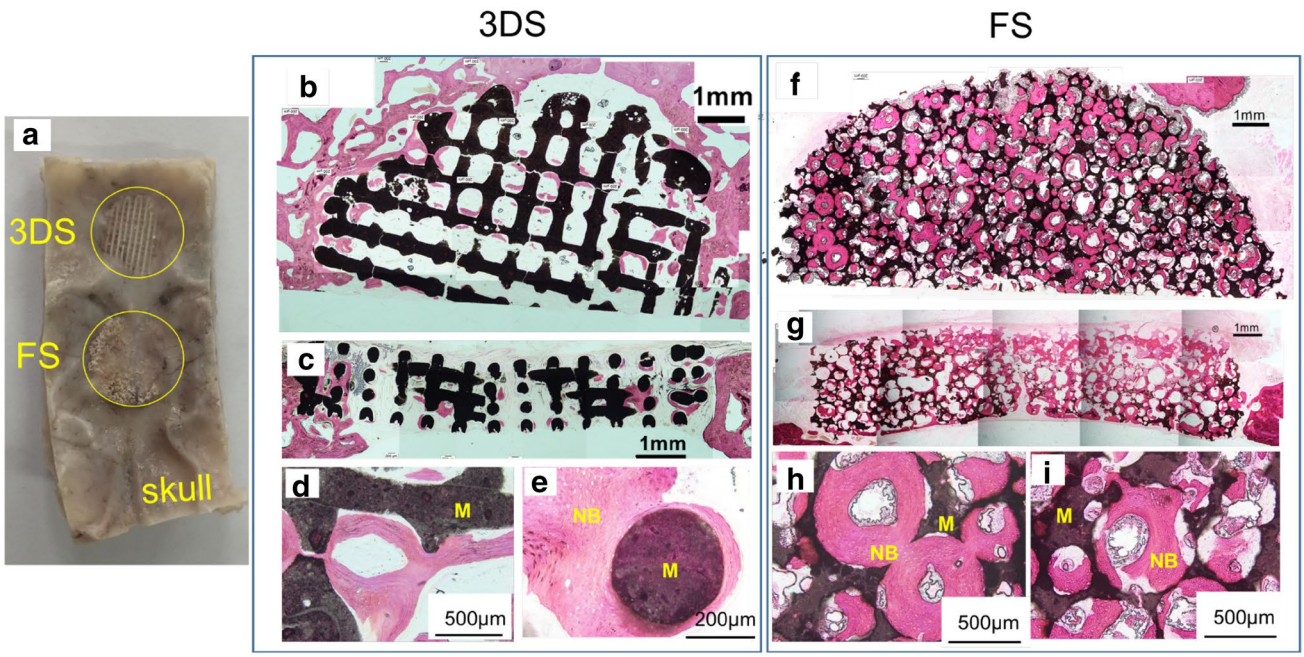

Fig. 6 New bone growth in 3DS and FS. **a** Photograph of the cross section of beagle skull containing 3DS and FS 5 months after implantation. **b**, **c** Gross hematoxylin and eosin (H&E) histological image of 5 months 3DS explants cross section. Black fiber is 3DS, and red part is bone. **d**, **e** H&E histological image of month 5 explants with 3DS fiber cross sections (dotted yellow letter) and new bone (yellow letter). **f**, **g** Gross hematoxylin and eosin (H&E) histological image of 5 months FS explants cross section. Black part is FS, and red part is bone. **h**, **i** H&E histological image of month 5 explants with FS cross sections (dotted yellow letter) and new bone (yellow letter)

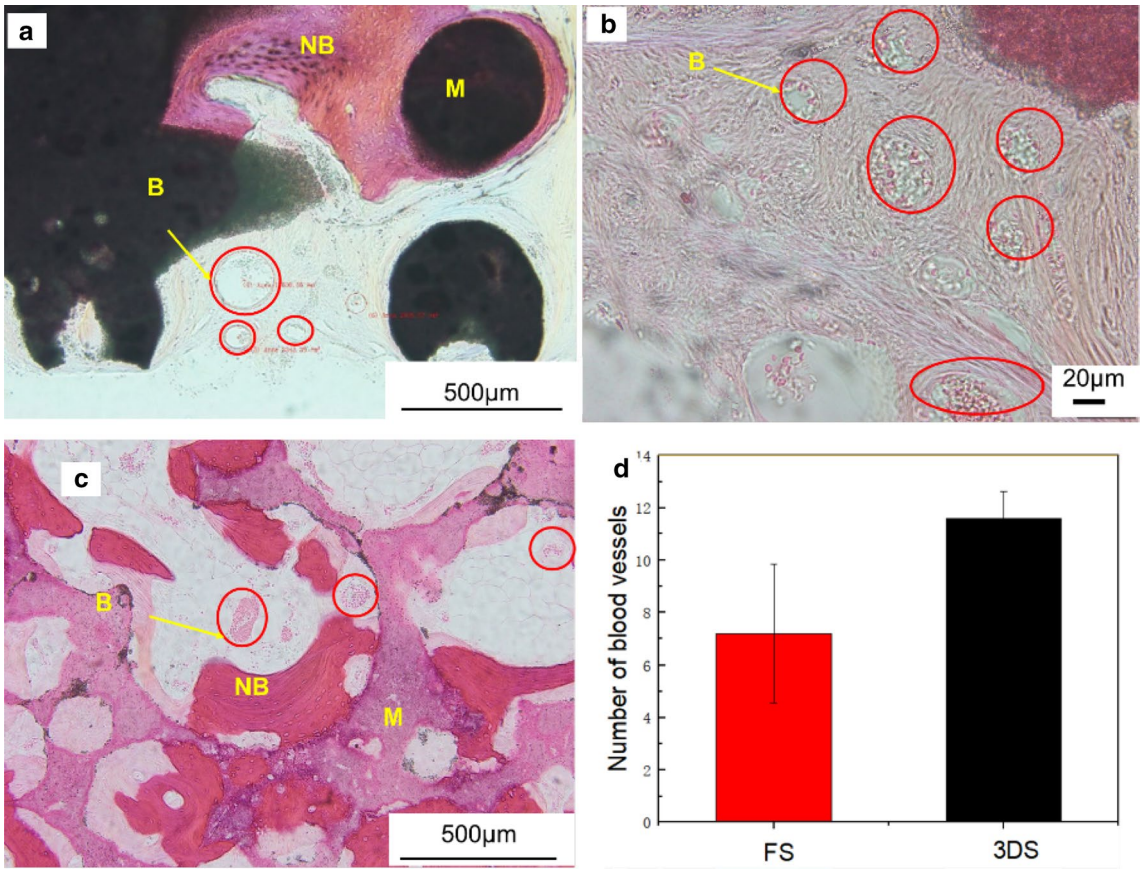

Fig. 7 Vascularization in 3DS and FS. **a** H&E histological image of month 5 explants with 3DS fiber cross sections (dotted yellow letter) and new bone (yellow letter) and vessels (solid red circles). **b** H&E histological high magnification image of month 5 explants with 3DS; some vessels were marked with solid red circles. **c** Histological image of month 5 explants with FS. **d** Statistically based quantification of new blood vessels per 2.5 mm^2 in 3DS and FS

the magnification image of 3DS (Fig. 7b), there were many blood vessels in the soft tissue inside the scaffold space. The vascular features showed fusiform, round or tubular, and the vessel wall is neatly sectioned with red blood cells inside. In comparison, the number of blood vessels in the FS is small. According to statistics, the number of blood vessels per 2.5 mm^2 is shown in Fig. 7e. It indicated that the number of blood vessels in the 3DS was significantly more than that of the FS. These blood vessels may provide nutrients and transportation of metabolic waste; it will help the bone repair in the later stages.

Discussion

Effect of the composition and structures on the degradation of 3D printing Ca-P ceramics

Personalized repair requires precise dimension implants. At present, direct 3D printing technology can only be used to prepare ceramic green bodies, which actually will shrink after sintering and resulting in an error between the design models and the printed scaffolds. Therefore, the design models should be scaled up according to the shrinkage before and after sintering of the ceramic to prepare the required scaffolds. After a large number of measurements, the shrinkage rate of calcium–phosphorus ceramic in this study was about 22% in linear direction. It should be noted that the horizontal shrinkage is slightly greater than that of longitudinal direction, which may be because of the slight compression of the material under the action of gravity during the printing process.

Calcium phosphate shows excellent osteoconductive and osteoinductive and is a promising bone repair biomaterial. In this paper, the degradation rate of the scaffold was controlled by adjusting the porous structure and the material composition, which may tailor the biodegradation rate to match the growth rate of new bone regeneration. In previous studies, it was proved that idea degradation rate of the implants helped bone repair. 3D printing technology can accurately control the pore structure and material composition of the scaffolds, so that it can design and tailor the degradation rate

of the scaffold. Smaller the diameter of the filament inside the scaffold caused faster degradation rate of the scaffold. In this study, we have prepared different porosity scaffolds, and the scaffolds with larger pores show higher porosity (Fig. 3), which theoretically corresponds a faster degradation rate. However, increase in porosity led to decrease in mechanical properties. We have determined the relationship between porosity and compressive strength, when the porosity was 60%, 70% and 80%; the compressive strength was 5.5 MPa, 3.0 MPa and 1.0 MPa, respectively. The compressive strength is much lower than the compact bone, which is just close to the mechanical requirements of cancellous bones. The increased compressive strength is limited for the porous BCP bioceramics by direct 3D printing technology. 3D printing technology is used as a forming technology to design and prepare the macroscopic structure of materials, but the final mechanical properties of ceramics depend on the property and inherent properties of the printing material. Although calcium phosphate ceramics show excellent bioactivity and osteoinductive properties, their mechanical strength and fracture toughness are relatively low. So, this type of material cannot be used for load-bearing bone defects. It is mainly used as a filler and coating. 3D printing strategy provides the possibility to design a porous scaffold with different degradation rates according to different bone repair requirements. A scaffold with a gradient pore structure can be designed to realize the gradient degradation of scaffold to meet gradient degradation application as shown in Fig. 1b.

Ca-P with different phase compositions showed different solubility. Hydroxyapatite has lowest solubility and hardly degrades in vivo, while the degradation rate of tricalcium phosphate is too fast to retain a temporary mechanical support for implantation duration. Therefore, a composite mixture consisting of HA and TCP was able to achieve an optimum solubility. From the phase composition and solubility study, as well as the comparison of osteoinductivity, it founded that a higher solubility of Ca-P ceramics results in higher osteoinductivity. These results are consistent with previous literature reports; the trend of osteoinductivity is BCP > β-TCP > HA > α-TCP [5, 39, 40]. Therefore, this research provided a 3D printing strategy to regulate the degradation rate of bioceramic by regulating different its components. Various formulations of calcium phosphate, i.e., different proportions of HA and TCP, have been successfully used in clinic; it depends on what kind of their degrade rate is needed [39–41]. Although the clinically used BCP is usually composed of nearly 60–70% HA and 30–40% β-TCP, the BCP consisting of 30% HA and 70% β-TCP promoted higher expression of bone morphogenetic protein-2 (BMP-2) and showed stronger osteoinductivity in mice than BCP (70% HA and 30% b-TCP), pure b-TCP and HA [42]. The BCP (70% β-TCP and 30% HA) degraded faster than the BCP consisting of 30% β-TCP and 70% HA, and is more suitable for defect that requires rapid degradation rate of the implants. This study only provides a way to regulate the degradation rate of calcium phosphate ceramics through 3D printing method. The specific formulation of calcium phosphate ceramics depends on the requirements of clinical application.

Regeneration of the skull

Although calcium phosphate ceramics show excellent bioactivity and osteoinductive properties, their mechanical strength and fracture toughness are relatively low. This type of material cannot be used for load-bearing bone defects. It is mainly used as a filler and coating. This research actually simulates the surgical procedure and proves its feasibility application in craniofacial and maxillofacial regeneration, which is conducive to the promotion and application of 3D printed ceramics. The skull model of the target animal was first obtained by CT, and a circular defect was created. Then according to the defect shape, the corresponding implant model was designed by computer and the ceramic scaffolds were prepared by 3D printing technology. Therefore, the 3DS was closely combined with the surrounding tissue after implantation and was more suitable for the original skull curve. It satisfied the aesthetic requirements of the craniofacial repair. The new bone tissue grew along the surface of the scaffold to the center; new bones were found at outer perimeter of the 3DS. There was isolated new bone tissue inside the scaffold. This part of the bone tissue was not combined with the surrounding bone tissue. It may be the induced new bones. The circular pores of the gas-foamed ceramic (FS) were full of new bone tissues.

In addition to the influence of the phase composition of the material, the porous structure of the scaffold also plays a key role in biological activity. Ripamonti et al. made a concave pore with a diameter of 1.6 mm and a depth of 0.8 mm on the surface of the HA. After implanting it into the baboon muscle for 90 days, only new bone formation in the concave pore of the implant was found [43]. It is indicated that the concave pore facilitates the formation of new bone. The pore structure affects the aggregation state of the cells, which in turn affects the activity of the material. The proposed scaffolds have spherical concave porous structure which may be beneficial to the growth of new bone. In addition, the pore size of natural bone tissue ranges from millimeters to nanometers. The scaffolds with a series of hierarchical porosity within the micron range could mimic the hierarchically porous structures of natural bones and promote regeneration of new bone. In bone tissue engineering, the vascularization is one of the most important of components. A larger number of new blood vessels were found in 3DS (Fig. 7), indicating that a highly

interconnect pore structure possibly facilitates the growth of blood vessels. These vessels may help in regeneration of new bones.

Although autologous bone is the best active material for bone repair, autologous bone still has limitations, and it must be in close contact with the original bone tissue to be successfully repaired. In this surgery study, it may be due to the excessive gap of the original implanted autologous bone and surrounding tissue, and the autologous bone repair group showed poor reconstruction results. 3D printing technology can print the scaffolds with accurate dimension matched with the defect sizes. In addition, 3D printing can be used for fabrication of macroporous structures of scaffolds, but 3D printing technology is still unable to obtain microstructures smaller than 10 μm due to the print nozzle accuracy. Therefore, the final hierarchical porosity of ceramic depends on the optimization of the material composition design and post-sintering process.

Conclusions

3D printing technology provides a versatile strategy to fabricate Ca-P ceramics with accurate shape to match the defect and tailored biodegradation rate to support bone regeneration. The raw materials used in this study are the Ca-P powders with good bone regeneration ability; by using the 3D printing technology, the porous structures and phase composition of the scaffold can be well controlled and tailor the degradation rate. The 3D printed Ca-P ceramic with required geometry and size is good for developing patient-tailored implants. The mechanical properties of the scaffolds can meet requirements for cancellous bone implantation. Based on clinical surgical cases, a personalized skull defect repair was conducted and proved the possibility of regeneration of skull. Vascularization phenomena were observed in the 3DS scaffolds, which promoted bone regeneration in the later stage. This research provided a 3D printing strategy to regulate the degradation rate of bioceramic by regulating scaffolds composition and porous structures. It indicated that 3D printed Ca-P bioceramics with tailored biodegradation rate is a promising candidate for personalized skull bone tissue reconstruction.

Acknowledgements This work was supported by the National Key Research and Development Program of China (No. 18YFB1105600, 2018YFC1106800), National Natural Science Foundation of China (51875518), Sichuan Province Science & Technology Department Projects (2016CZYD0004, 2017SZ0001, 2018GZ0142, 2019YFH0079), Research Foundation for Young Teachers of Sichuan University (2018SCUH0017) and The "111" Project (No. B16033).

Compliance with ethical standards

Conflict of interest The authors declare that they have no conflict of interests.

Ethical approval The animal experiments were approved by the Animal Care and Use Committee of Sichuan University. All applicable international, national, and/or institutional guidelines for the care and use of animals were followed.

References

1. Song P, Hu C, Pei X, Sun J et al (2019) Dual modulation on crystallinity and macro/micro structures of 3D printed porous titanium implants to enhance the stability and osseointegration. J Mater Chem B. 7:2865–2877
2. Ahadian S, Khademhosseini A (2018) A perspective on 3D bioprinting in tissue regeneration. Bio-Des Manuf 1(3):157–160
3. Pei X, Ma L, Zhang B, Sun J, Sun Y, Fan Y et al (2017) Creating hierarchical porosity hydroxyapatite scaffolds with osteoinduction by three-dimensional printing and microwave sintering. Biofabrication 9(4):045008
4. Miao X, Hu Y, Liu J, Wong AP (2004) Porous calcium phosphate ceramics prepared by coating polyurethane foams with calcium phosphate cements. Mater Lett 58(3–4):397–402
5. Samavedi S, Whittington AR, Goldstein AS (2013) Calcium phosphate ceramics in bone tissue engineering: a review of properties and their influence on cell behavior. Acta Biomater 9(9):8037–8045
6. Zhang B, Pei X, Zhou C, Fan Y, Jiang Q, Ronca R et al (2018) The biomimetic design and 3D printing of customized mechanical properties porous Ti6Al4V scaffold for load-bearing bone reconstruction. Mater Des 152(15):30–39
7. Yuan HYZ, Li Y et al (1998) Osteoinduction by calcium phosphate biomaterials. J Mater Sci Mater Med 72:3–6
8. Woodard JR, Hilldore AJ, Lan SK, Park CJ, Morgan AW, Eurell JA et al (2007) The mechanical properties and osteoconductivity of hydroxyapatite bone scaffolds with multi-scale porosity. Biomaterials 28(1):45–54
9. Ripamonti U, Van den Heever B, van Wyk J (1993) Expression of the osteogenic phenotype in porous hydroxyapatite implanted extraskeletally in baboons. Biomaterials 17:491–502
10. Carrodeguas RG, De Aza S (2011) Alpha-tricalcium phosphate: synthesis, properties and biomedical applications. Acta Biomater 7(10):3536–3546
11. Hirota M, Hayakawa T, Shima T, Ametani A, Tohnai I (2015) High porous titanium scaffolds showed higher compatibility than lower porous beta-tricalcium phosphate scaffolds for regulating human osteoblast and osteoclast differentiation. Mater Sci Eng C Mater Biol Appl. 49:623–631
12. Mohammadi Z, Sheikh-Mehdi Mesgar A, Rasouli-Disfani F (2016) Preparation and characterization of single phase, biphasic and triphasic calcium phosphate whisker-like fibers by homogenous precipitation using urea. Ceram Int 42(6):6955–6961
13. Yuan H, Li Y, Feng Z, Yang K, de Groot K, Zhang X (2001) Bone formation induced by calcium phosphate ceramics in soft tissue of dogs: a comparative study between porous a-TCP and b-TCP. J Mater Sci Mater Med 12:7–13
14. Zhu Y, Zhang K, Zhao R, Ye X, Chen X, Xiao Z et al (2017) Bone regeneration with micro/nano hybrid-structured biphasic calcium phosphate bioceramics at segmental bone defect and the induced immunoregulation of MSCs. Biomaterials 147:133–144

15. Marques CF, Perera FH, Marote A, Ferreira S, Vieira SI, Olhero S et al (2017) Biphasic calcium phosphate scaffolds fabricated by direct write assembly: mechanical, anti-microbial and osteoblastic properties. J Euro Cera Soci 37(1):359–368
16. Wang Z, Tang Z, Qing F, Hong Y, Zhang X (2012) Applications of calcium phosphate nanoparticles in porous hard tissue engineering scaffolds. NANO 07(04):1230004–1230018
17. Kim HJ, Park IK, Kim JH, Chong SC, Kim MS (2012) Erratum to: gas foaming fabrication of porous biphasic calcium phosphate for bone regeneration. Tissue Eng Regen Med 9(4):232
18. Tang Z, Li X, Tan Y, Fan H, Zhang X (2018) The material and biological characteristics of osteoinductive calcium phosphate ceramics. Regen Biomater 5(1):43–59
19. Perez RA, Mestres G (2016) Role of pore size and morphology in musculo-skeletal tissue regeneration. Mater Sci Eng C Mater Biol Appl 61:922–939
20. Phadke A, Hwang Y, Hee Kim S, Hyun Kim S, Yamaguchi T, Masuda K et al (2013) Effect of scaffold microarchitecture on osteogenic differentiation of human mesenchymal stem cells. Euro Cells Mater 25:114–129
21. Penk A, Forster Y, Scheidt HA, Nimptsch A, Hacker MC, Schulz-Siegmund M et al (2013) The pore size of PLGA bone implants determines the de novo formation of bone tissue in tibial head defects in rats. Magn Reson Med 70(4):925–935
22. Costa JB, Silva-Correia J, Reis RL, Oliveira JM (2018) Current advances in solid free-form techniques for osteochondral tissue engineering. Bio-Des Manuf 1(3):171–181
23. Jeong CG, Hollister SJ (2010) Mechanical and biochemical assessments of three-dimensional poly(1,8-octanediol-co-citrate) scaffold pore shape and permeability effects on in vitro chondrogenesis using primary chondrocytes. Tissue Eng A 16(12):3759–3768
24. Kujala S, Ryhänen J, Danilov A, Tuukkanen J (2003) Effect of porosity on the osteointegration and bone ingrowth of a weight-bearing nickel–titanium bone graft substitute. Biomaterials 24(25):4691–4697
25. Meza LR, Zelhofer AJ, Clarke N, Mateos AJ, Kochmann DM, Greer JR (2015) Resilient 3D hierarchical architected metamaterials. Proc Natl Acad Sci USA 112(37):11502–11507
26. Fukasawa T, Ando M, Ohji T, Kanzaki S (2001) Synthesis of porous ceramics with complex pore structure by freeze-dry processing. J Am Ceram Soc 84(1):230–232
27. Liu R, Xu T, Wang CA (2016) A review of fabrication strategies and applications of porous ceramics prepared by freeze-casting method. Ceram Int 42(2):2907–2925
28. Wu SC, Hsu HC, Hsiao SH, Ho WF (2009) Preparation of porous 45S5 Bioglass® -derived glass–ceramic scaffolds by using rice husk as a porogen additive. J Mater Sci Mater Med 20(6):1229
29. Ray AML, Gautier H, Bouler JM, Weiss P, Merle C (2010) A new technological procedure using sucrose as porogen compound to manufacture porous biphasic calcium phosphate ceramics of appropriate micro- and macrostructure. Ceram Int 36(1):93–101
30. Wang XX, Li W, Kumar V (2006) A method for solvent-free fabrication of porous polymer using solid-state foaming and ultrasound for tissue engineering applications. Biomaterials 27(9):1924–1929
31. Moghadam MZ, Hassanajili S, Esmaeilzadeh F, Ayatollahi M, Ahmadi M (2017) Formation of porous HPCL/LPCL/HA scaffolds with supercritical CO_2 gas foaming method. J Mech Behav Biomed Mater 69:115–127
32. Jing X, Mi HY, Turng LS (2017) Comparison between PCL/hydroxyapatite (HA) and PCL/halloysite nanotube (HNT) composite scaffolds prepared by co-extrusion and gas foaming. Mater Sci Eng C Mater Biol Appl 72:53–61
33. Jakus AE, Rutz AL, Jordan SW, Kannan A, Mitchell SM, Yun C et al (2016) Hyperelastic "bone": a highly versatile, growth factor-free, osteoregenerative, scalable, and surgically friendly biomaterial. Sci Trans Med 8(358):15
34. Wang X, Ao Q, Tian X, Fan J, Wei Y, Hou W et al (2016) 3D Bioprinting technologies for hard tissue and organ engineering. Materials 9(10):23
35. Chen Z, Li Z, Li J, Liu C, Lao C, Fu Y et al (2019) 3D printing of ceramics: a review. J Euro Ceram Soc 39(4):661–687
36. Bose S, Vahabzadeh S, Bandyopadhyay A (2013) Bone tissue engineering using 3D printing. Mater Today 16(12):496–504
37. Hwa LC, Rajoo S, Noor AM, Ahmad N, Uday MB (2017) Recent advances in 3D printing of porous ceramics: a review. Curr Opin Solid State Mater Sci 21(6):323–347
38. Zhang B, Pei X, Song P, Sun H, Li H, Fan Y et al (2018) Porous bioceramics produced by inkjet 3D printing: effect of printing ink formulation on the ceramic macro and micro porous architectures control. Compos B Eng 155:112–121
39. Wang J, Chen Y, Zhu X, Yuan T, Tan Y, Fan Y et al (2015) Effect of phase composition on protein adsorption and osteoinduction of porous calcium phosphate ceramics in mice. J Biomed Mater Res A 102(12):4234–4243
40. Ji K, Wang Y, Wei Q, Zhang K, Jiang A, Rao Y et al (2018) Application of 3D printing technology in bone tissue engineering. Bio-Des Manuf 1(3):203–210
41. Shao H, Yang X, He Y, Fu J, Liu L, Ma L, Zhang L, Yang G, Gao C, Gou Z (2015) Bioactive glass-reinforced bioceramic ink writing scaffolds: sintering, microstructure and mechanical behavior. Biofabrication 7(3):035010
42. Wang J, Chen Y, Zhu X, Yuan T, Tan Y, Fan Y et al (2014) Effect of phase composition on protein adsorption and osteoinduction of porous calcium phosphate ceramics in mice. J Biomed Mater Res A 102(12):4234–4243
43. Ripamonti U (1991) Bone induction in nonhuman primates. An experimental study on the baboon. Clin Orthop Relat Res 269:284–294